Applied Surface Science 579 (2022) 152145

Contents lists available at ScienceDirect

Applied Surface Science

journal homepage: www.elsevier.com/locate/apsusc

Full Length Article

Critical comparison of aerogel TiO_2 and P25 nanopowders: Cytotoxic properties, photocatalytic activity and photoinduced antimicrobial/antibiofilm performance

Guru Karthikeyan Thirunavukkarasu [a], Jana Bacova [b], Olivier Monfort [a], Ewa Dworniczek [c], Emil Paluch [c], Muhammad Bilal Hanif [a], Sajid Rauf [d], Monika Motlochova [e], Jan Capek [b], Karol Hensel [f], Gustav Plesch [a], Grzegorz Chodaczek [g], Tomas Rousar [b,*], Martin Motola [a,*]

[a] Department of Inorganic Chemistry, Faculty of Natural Sciences, Comenius University in Bratislava, Ilkovicova 6, Mlynska Dolina, Bratislava 842 15, Slovakia
[b] Department of Biological and Biochemical Sciences, Faculty of Chemical Technology, University of Pardubice, Pardubice 532 10, Czech Republic
[c] Department of Microbiology, Faculty of Medicine, Wroclaw Medical University, Wroclaw 50-368, Poland
[d] College of Electronics and Information Engineering, Shenzhen University, Guangdong Province, 518000, China
[e] Institute of Inorganic Chemistry, Czech Academy of Sciences, Husinec-Rez 1001, Rez 250 68, Czech Republic
[f] Division of Environmental Physics, Faculty of Mathematics, Physics and Informatics, Comenius University in Bratislava, Mlynska Dolina, Bratislava 842 48, Slovakia
[g] Łukasiewicz Research Network - PORT Polish Center for Technology Development, Bioimaging Laboratory, Stabłowicka 147, Wrocław 54-066, Poland

ARTICLE INFO

Keywords:
TiO_2
Toxicity
Antimicrobial
Antibiofilm
Photocatalysis

ABSTRACT

A critical comparison of two TiO_2 nanopowders is herein presented. TiO_2 aerogel powder synthesized via lyophilization (TiAP) and commercially available TiO_2 Evonik (P25) are thoroughly investigated for their toxicity, photoinduced antimicrobial and antibiofilm properties, and photocatalytic activity. Time- and concentration-dependent A549 cell viability inhibition was characterized using estimating the mitochondrial dehydrogenase activity and glutathione levels. Both materials showed low toxicity in the pulmonary A549 cells. Photocatalytic activity of TiAP and P25 in the degradation of methylene blue and caffeine was determined, and TiAP was more efficient than P25 by 1.2–2.8 times. That is due to the 2D morphology of TiAP, along with an increased generation of hydroxyl radicals compared to a system containing 0D P25. Photoinduced antimicrobial and antibiofilm performance of TiAP and P25 on inactivation of gram-negative *E. coli* and gram-positive *E. faecalis* showed a complete log 6 reduction in the amount of bacteria after 60 min UV-A irradiation.

1. Introduction

Photocatalytic activity of TiO_2 was first reported in 1921 [1], and its use in chalking of paint is known from 1949 [2]. However, this unique material has received a significant interest after the pioneering work of Fujishima and Honda in 1972 [3] on catalytic water splitting under UV light irradiation. The photocatalytic activity of TiO_2 was further exploited for its ability to catalyze the oxidation of organic and inorganic pollutants in 1976 [4] and 1977 [5], respectively, and to kill microorganisms in 1985 [6]. Ever since, TiO_2 has gained a considerable attention due to its exceptional photoinduced properties. It includes killing of viruses [7] and bacteria [8] in water bodies, preventing biofilm formation in bioreactors [9], air-filters [10], potential killing of cancer cells [11], and treatment of waters [12–14]. Nowadays, TiO_2 is used as the material for outer/inner walls and windows of hospitals, commercial facilities, and hotels due to its function as a deodorizer with self-cleaning [15,16] and antibacterial [17,18] properties.

The photocatalytic mechanism on TiO_2 surfaces is based on photoinduced activation by incident UV light absorption, generation of charge carriers (e^-/h^+ pairs) and subsequent formation of reactive oxygen species (ROS), which react with the target molecules [19,20]. Concerning the photoinduced antimicrobial and antibiofilm activity, TiO_2 interacts with the cell membrane and is able to kill the microorganism via the action of ROS, thus leading to fragmentation of the cell membrane [21]. In addition, TiO_2 is able to kill the bacteria via cell fragmentation, i.e., by mechanical force that destroys the cell membrane [21,22].

To increase the efficiency of TiO_2 in photoinduced applications,

* Corresponding authors.
E-mail addresses: tomas.rousar@upce.cz (T. Rousar), martin.motola@uniba.sk (M. Motola).

https://doi.org/10.1016/j.apsusc.2021.152145
Received 14 October 2021; Received in revised form 26 November 2021; Accepted 4 December 2021
Available online 11 December 2021

several nanostructured TiO_2 materials in the form of powders (particles, fibers, nanotubes, etc.) or supported layers (thin films, supported nanotubes, etc.) were developed [19,23–31]. The design of optimal physico-chemical properties of TiO_2 such as crystal structure, surface area, and particle size are crucial [32–34]. Among the variety of TiO_2 nanostructured materials, nanopowders are promising as they possess the above-mentioned features and consist mainly of the anatase TiO_2 phase and possess a sufficient amount of surface hydroxyl groups [35,36]. Over the years, the commercially available TiO_2 Evonik (formerly Degussa) AEROXIDE® TiO_2 P-25 (P25) became a representative TiO_2 nanopowder. P25 is a multiphasic TiO_2 containing anatase and rutile (80:20 wt% ratio, respectively) prepared via pyrolysis [37]. Although a majority of the reports on photocatalytic and photoinduced antimicrobial activity describe P25 with lower efficiency compared to that of newly designed TiO_2 nanopowders, P25 remains an efficient photocatalyst with probably better economic advantages. P25 possesses remarkable properties such as high chemical purity, low aggregation and high quantum yield [38–40].

On the other hand, other techniques such as lyophilization (i.e., freeze-drying) can be employed for the preparation of TiO_2 nanopowders. This technique [35,41,42] offers an environmentally- and economically-friendly synthesis of TiO_2 in the form of aerogel powders (TiAP) with controllable particle size and phase composition and high specific surface area, although it is a time-consuming method that requires high vacuum. Our previous works [26,35,43] reported the preparation of TiAP with 2D morphology and their better photocatalytic efficiency than P25. However, toxicity and photoinduced antimicrobial and antibiofilm performance of such TiAP nanopowder (along with a comparison with P25) has not been yet reported. As prognosed by Robichaud et al. [44], the annual global production of 14 million tons of TiO_2 as a basis for exposure assessment will be reached by 2025. Thus, it is necessary to comprehensively study TiO_2 nanopowders (both commercially available P25 and newly-prepared TiAP) in different photoinduced applications and to critically assess their efficiency.

In the present work, we thoroughly investigated the photoinduced catalytic, antimicrobial, and antibiofilm properties along with the toxicity of two different TiO_2 nanopowders (i.e., TiAP and P25) prepared by different methods (i.e., pyrolysis and lyophilization). The toxicity assessments in A549 pulmonary cells were first evaluated. As second, photocatalytic degradation of two model organic pollutants (methylene blue and caffeine) was conducted in pure water and physiological solution, respectively. At last, photoinduced antimicrobial and antibiofilm activity was evaluated on *Enterococcus faecalis* (planktonic form and biofilm) and *Escherichia coli* (planktonic form) as target bacteria. Such comprehensive study of TiO_2 nanopowders is critically discussed to highlight the advantages and the drawbacks of both P25 and TiAP. It also opens the door for future applications in the disinfection of bacteria-rich environments such as hospitals and hotels and the removal of organic pollutants in wastewaters.

2. Experimental part

2.1. Nanopowders synthesis and characterization

Two different types of TiO_2 nanopowders were used in this study: 1) TiO_2 aerogel powders (TiAP) and 2) commercially available TiO_2 evonik (P25). The preparation of TiAP was prepared via the freeze-drying method (i.e., lyophilization), which is reported in our previous works [43,45], and it is briefly described in Electronic Supplementary Information (ESI).

Morphology and phase composition was determined via Scanning Electron Microscopy (SEM, Tescan Lyra III) and X-ray Diffraction (XRD, PANalytical) using a Cu K_α radiation ($\lambda = 1.5418$ Å), respectively, while the Brunauer-Emmett-Teller method was used to calculate the specific surface area via a cylindrical pore model [46].

2.2. Cell culture preparation and cytotoxicity assessment

The human lung carcinoma epithelial cells (A549) were obtained from ATCC (CCL-185, Manassas, VA, USA) and cultured according to recommended conditions. The cells were proven to be Mycoplasma-free, and the origin of the cells was confirmed by short tandem repeats analysis.

For cytotoxicity assay, TiAP and P25 nanoparticles were suspended in culture medium to obtain stock solutions (1 $mg.mL^{-1}$) and diluted to final concentrations (1; 10 and 100 $\mu g.mL^{-1}$). The endotoxin contamination of the powder materials was tested using the PyroGene™ Recombinant Factor C Assay (Lonza, Blackley, UK).

Briefly, A549 cells were seeded in 96-well plates at density of $5x10^3$ cells per well overnight. After seeding, cells were exposed to the TiAP and P25 nanoparticles. The cells were incubated with materials for 24 h and 48 h. Untreated cells were used as a negative control. 100 $\mu g.mL^{-1}$ multiwalled carbon nanotubes (MWCNT, JRC Nanomaterials repository, Ispra, Varese, Italy) were established as a positive control.

After the treatment with TiAP and P25 nanoparticles, the cytotoxicity assessment on A549 cells was assessed using the WST-1 test (Sigma-Aldrich, USA) and glutathione asay. The WST-1 test detects the activity of mitochondrial dehydrogenases. After exposure, the cells were incubated with the WST-1 reagent for 1 h. The change of absorbance (0–1 h) was measured at the wavelength of 440 nm using a microplate reader (Tecan SPARK, Austria). The dehydrogenase activity was expressed as the percentage of total cellular dehydrogenases activity relative to that in untreated cells (control = 100%). Glutathione (GSH) levels were measured using an optimized bimane assay [47]. The fluorescence intensity ($\lambda_{ex}/\lambda_{em}$ = 394/490 nm) was measured kinetically for 20 min using SPARK microplate reader (Tecan, Austria). The fluorescence was expressed as the slope of a fluorescence change over time. The GSH levels were expressed as the percentage relative to the GSH levels in untreated cells (control = 100%). We evaluated the occurrence of nanopowder interference with WST-1 and GSH assays. All tested materials were found to cause no significant interference in both tests. The background signal was always under 5% of that in untreated cells.

For microscopy, A549 cells were seeded at a density of 10×10^3 cells/well of a chamber slide. After 24 h, the cells were exposed to TiAP and P25. After 24 h of treatment, cells were fixed with formaldehyde, permeabilized with Triton X 100 and washed with phosphate-buffered saline. Fluorescence probes were used to visualize the cells: Hoechst 33258 (Sigma-Aldrich, USA) to stain cell nucleus and phalloidin-TRITC (=tetramethylrhodamine B isothiocyanate, Sigma-Aldrich, USA) to stain actin filaments. The actin filaments (TRITC filter, 540/25 nm) and cell nuclei (DAPI filter, 375/28 nm) were observed with a fluorescence microscope (Nikon Eclipse 80i, Japan).

All experimental procedures with pulmonary cells were repeated three times independently with at least four replicates. The results are expressed as a mean ±S.D. The Analysis of Variance followed by Bonferroni post-test was used to perform the mean comparison at significance level $p = 0.05$ (*, $p < 0.05$, **, $p < 0.01$, ***, $p < 0.001$).

2.3. Photocatalytic activity and HO• radicals production

The photocatalytic activity was evaluated by monitoring the degradation of model organic pollutants, i.e., methylene blue aqueous solution (MB, initial concentration c = 10 μM, 99+%, Acros Organics) and caffeine aqueous solution (CAF, initial concentration c = 20 ppm, ReagentPluss, Sigma-Aldrich) under solar-like irradiation (metal-halogen arc-lamp, HQI TS-OSRAM 400 W/D6500K with a UVB pyrex filter, λ_{max} = 365 nm, 0.73 $mW.cm^{-2}$ in the range 335–380 nm) with constant air bubbling and magnetic stirring in a self-constructed apparatus [48]. All the photocatalytic experiments were performed using 0.1 $mg.L^{-1}$ of suspended TiO_2 nanopowder in 30 mL of an aqueous solution containing the pollutant. To achieve adsorption/desorption equilibrium, the mixture was placed for 1 h in the dark. The degradation of MB and

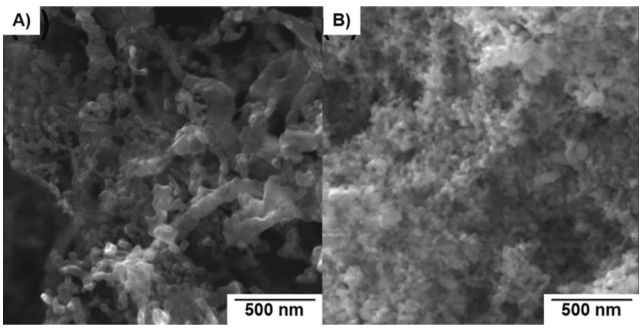

Fig. 1. SEM images of TiO_2 nanopowders: A) TiAP and B) P25.

CAF was estimated from the decrease of the maximum absorbance at 670 nm and 270 nm, respectively, using a UV–VIS spectrophotometer (Jasco V-530). The photocatalytic experiments were performed in both distilled water and physiological solution (0.85% NaCl) in order to better assess the photocatalytic efficiency at conditions approaching those in biomedical applications. In addition, the majority of the photoinduced antimicrobial and antibiofilm properties are evaluated in physiological solutions. During the measurement, the mixture was sampled out at a predetermined time, and the supernatant was collected by centrifugation and subsequently analysed.

2.4. Antimicrobial properties of TiAP and P25 on planktonic forms of Enterococcus faecalis and Escherichia coli

Strains of *Enterococcus faecalis* 37VRE and *Escherichia coli* PA1 were used as representative microorganisms to measure the photoinduced antimicrobial properties of TiAP and P25. The bacterial solutions (1.0×10^6 CFU.mL^{-1}; colony forming unit per one milliliter) were mixed with TiAP and P25 in 0.85% NaCl to achieve final concentrations of 1500 μg.mL^{-1}, 750 μg.mL^{-1}, 375 μg.mL^{-1}, 188 μg.mL^{-1}, and 94 μg.mL^{-1}.

Prior to light exposition, reaction suspension was continually stirred for 60 min at room temperature (RT). Then, half of the sample was exposed to UV-A light in the perpendicular direction with the Wood's lamp ($\lambda = 365$ nm, 11 mW.cm^{-2}), whereas the other half was kept in the dark. At the given time intervals (0 min, 15 min, 30 min, and 60 min), 100 μL aliquots of each reaction suspension was withdrawn, diluted and a 50 μL aliquot was spread onto Tryptic Soy agar (TSA, Biomaxima, Poland) plates. After 24–48 h incubation at 37 °C, the number of colonies was counted. The bactericidal activity of TiAP and P25 was evaluated by comparing the value of $\log_{10}$ CFU.mL^{-1}. The data and conclusions were confirmed by replicate experiments.

2.5. Effect of TiAP and P25 on mature biofilms of Enterococcus faecalis and study of biofilm formation in the microfluidic flow system

The mature 24 h biofilms of *E. faecalis* were exposed to the TiAP and P25 suspensions at final concentration of 188 μg.mL^{-1}. Biofilms in 0.85% NaCl and biofilms treated with 70% ethanol were used as negative and positive controls, respectively. One sample set of control biofilms and TiAP and P25 treated biofilms was UV-A irradiated for 60 min. A similar sample set was maintained in the dark camera for 60 min as a non-irradiated reference. Then all biofilms were stained with FilmTracerTM LIVE/DEADTM Biofilm Viability Kit (ThermoFisher Scientific) and evaluated by an upright Leica SP8 resonant scanning confocal system (Leica Microsystem, Germany). The percentage of dead cell area in the biofilms was determined using ImageJ software (NIH). The combined signal from Syto 9 and PI was also quantified to determine the total biomass area (live + dead) [49].

The BioFlux1000 system, with 48-well plates (Fluxion Biosciences, California, USA), was used to study biofilm formation in continuous flow. After the photocatalytic inactivation as described above, the planktonic *E. faecalis* cells, were flushed into the channels of the BioFlux plate and incubated for 24 h. The biofilms were stained with LIVE/DEAD™ BacLight™ Bacterial Viability Kit (Invitrogen, USA) and imaged with a 1 h intervals. Quantification of fluorescence was performed with the BioFlux software (Fluxion, USA) [50]. The biofilm viability was calculated based on the formula shown in ESI. Moreover, ESI provides a more detailed information regarding the Experimental part.

2.6. Detection of aqueous and intracellular ROS (HO• and iROS)

In an aqueous solution, the production of HO• by TiAP and P25 was studied by the terephthalic acid assay using fluorescence spectroscopy (Shimadzu RF-6000). In typical produce, samples (0.1 mg.mL^{-1}) were suspended in 30 mL aqueous solution of terephthalic (TA, 2 mM) and kept in the dark for 30 min. After the mixture is exposed to solar-like irradiation, thereby generating HO• which reacts with TA to form fluorescent hydroxy terephthalate ($\lambda_{ex} = 310$ nm and $\lambda_{em} = 425$ nm).

Total (HO• and O_2•-) intracellular reactive oxygen species (iROS) levels were measured using the 5 μM CellROXTM Green Reagent (Invitrogen by Thermo Fisher Scientific, Eugene, Oregon, USA). Additionally, the 5 μM dihydroethidium (DHE) probe (Sigma-Aldrich, St Louis, USA) was used to quantify the amount of intracellular superoxide anion (O_2•-). The bacteria (10^8 CFU.mL^{-1}) with H_2O (1 mL:1 mL) and bacteria with 1.5% H_2O_2 were used as a negative and positive controls, respectively.

The fluorescence values of control and treated (188 μg.mL^{-1} of TiAP and P25, 60 min, UV-A/dark) cells were measured in 96-well black titration plates (Thermo Fisher Scientif, Roskilde, Denmark) using a

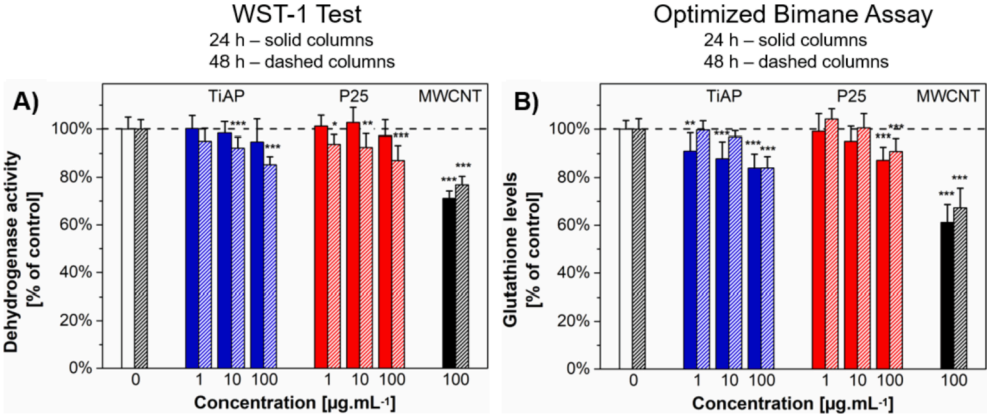

Fig. 2. The effect of TiAP and P25 (1, 10, 100 μg.mL^{-1}) on A) dehydrogenase activity and B) glutathione levels in A549 pulmonary cells after 24 h and 48 h. MWCNT (100 μg.mL^{-1}) were used as a positive control. Data are expressed as % of untreated cells (i.e., control) and represent the mean ± SD of three independent experiments. *, $p < 0.05$; **, $p < 0.01$; ***, $p < 0.001$ (vs. untreated cells).

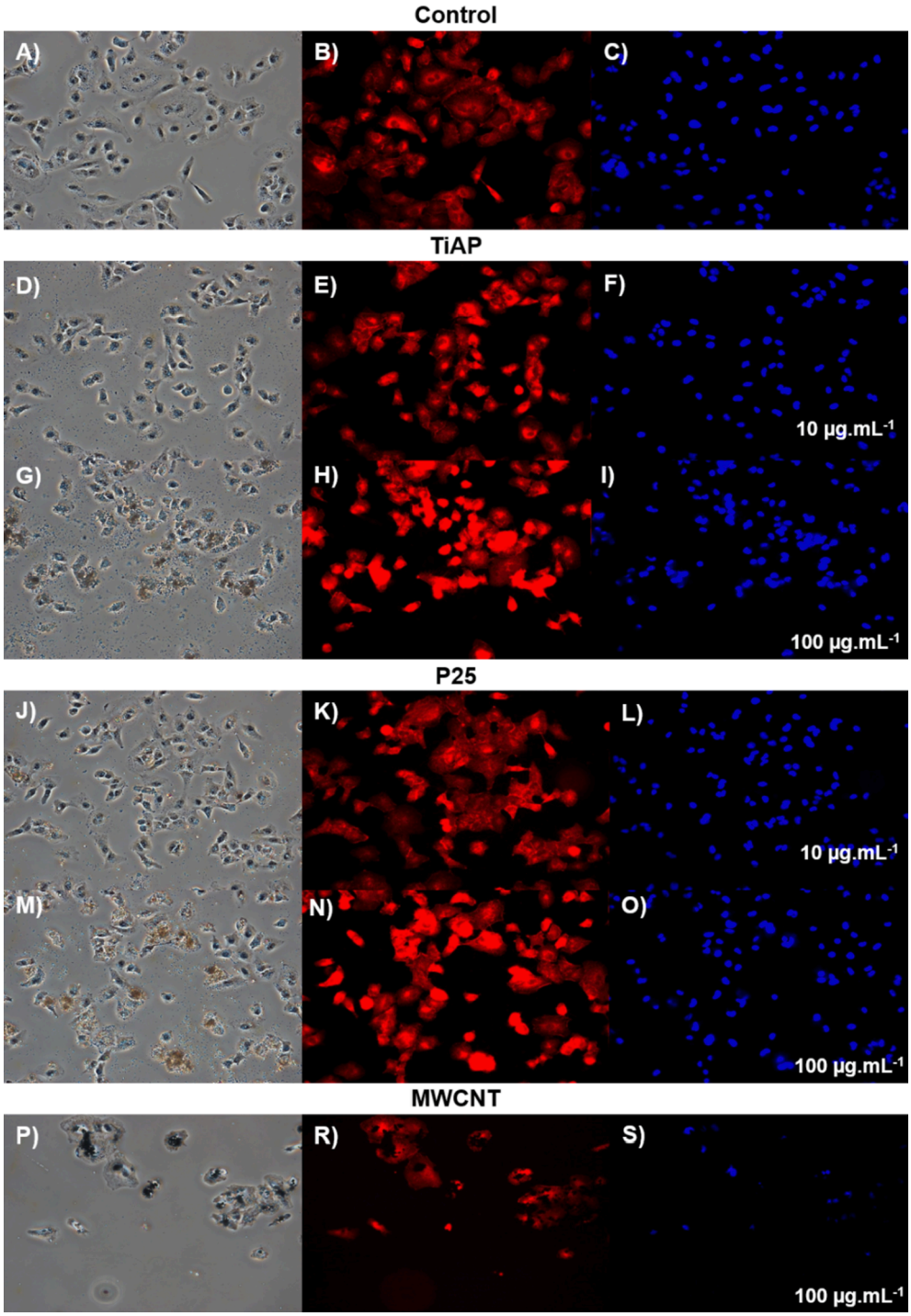

Fig. 3. Photomicrographs of A549 pulmonary cells grown for 24 h: untreated (*A-C*), TiAP (10 and 100 µg.mL^{-1}; *D-I*), P25 (10 and 100 µg.mL^{-1}; *J-O*), and MWCNT (100 µg.mL^{-1}; *P-S*). The cells were stained to visualize actin filaments (red, phalloidin-TRITC) and cell nuclei (blue, Hoechst 33258).

microplate reader (Infinite M200PRO, Tecane, Switzerland) with the excitation/emission wavelengths of 485 nm/520 nm for CellROXTM Green Reagent and 480 nm/590 nm for DHE probe. Relative ROS levels were calculated by the fluorescence ratio of the treatments to the control, in triplicate [51].

3. Results and discussion

3.1. Structural properties

Fig. 1A and B shows representative SEM images of TiAP and P25, respectively. TiAP possess 2D morphology whereas P25 a 0D one. The 2D structure of TiAP was previously confirmed by our group [26,43,52] and additional FESEM and TEM images that confirm the 2D structure of TiAP are shown in ESI (Fig. S2). Both materials are prone to form agglomerates due to their powder nature with crystallite size of < 40 nm. The crystallite size observed on SEM images is in good correlation with the crystallite size calculated from XRD (Fig. S1). Indeed, using the Debye-Scherrer equation for the (1 0 1) diffraction of the anatase TiO_2, the average crystallite size is approx. 32 nm and 20 nm for TiAP and P25, respectively. A decrease in the average crystallite size for P25 compared to that of TiAP is due to the different preparation techniques, i.e.,

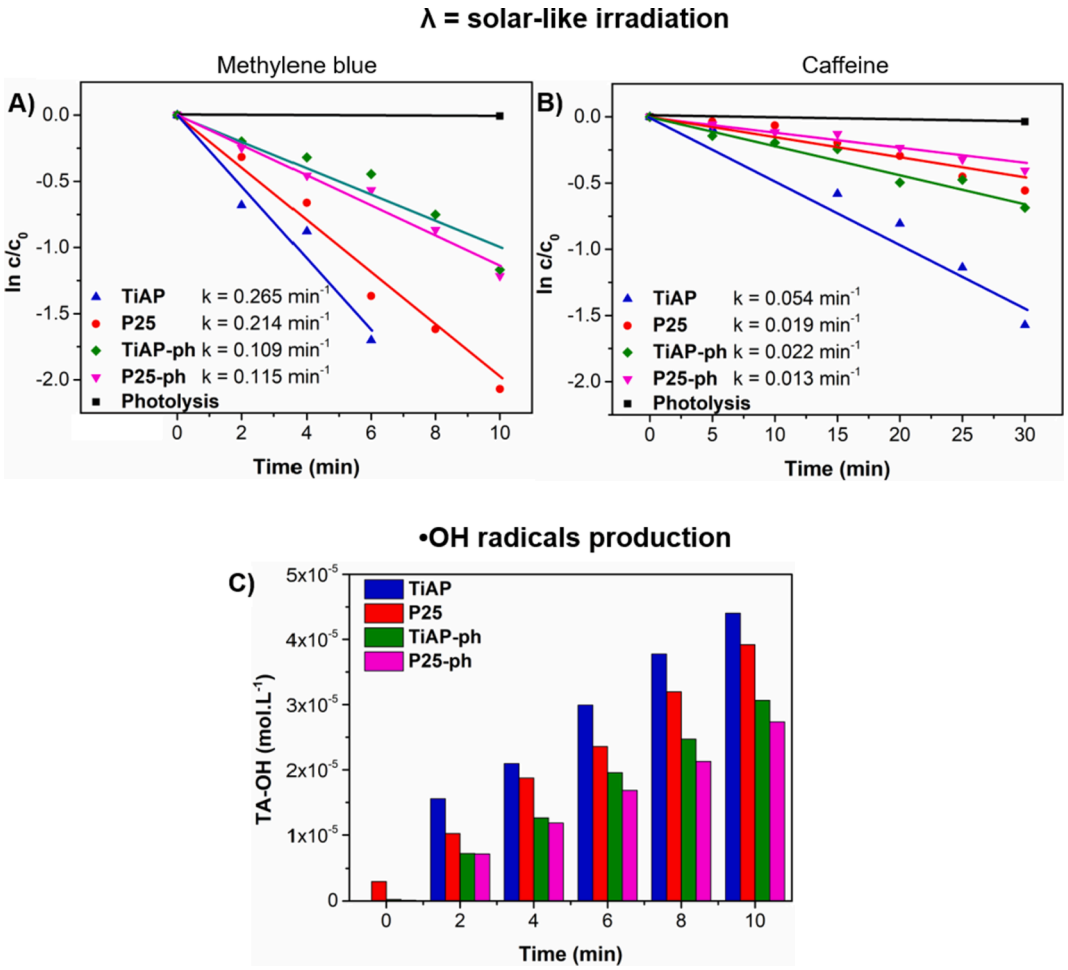

Fig. 4. Photocatalytic degradation rates of A) Methylene blue and B) Caffeine in aqueous (*X*) and physiological (*X-ph*) solution for TiAP (TiAP and TiAP-ph, respectively) and P25 (P25 and P25-ph, respectively) under solar-like irradiation. *k* represents the calculated first-order kinetic rate constant. C) Dependence overtime of the concentration of hydroxyl-terephthalic acid (TA-OH) produced during solar-like irradiation of TiAP, P25, TiAP-ph, and P25-ph, respectively.

pyrolysis for P25 and lyophilization for TiAP. Consequently, a higher specific surface area was obtained for P25 (S_{BET} = 35.4 $m^2.g^{-1}$) compared to that of TiAP (S_{BET} = 15.6 $m^2.g^{-1}$) since a smaller crystallite size usually leads to a higher specific surface area. In addition, the optical bandgap (E_g) was calculated using the Tauc's plot from diffuse reflectance spectra (Fig S3) for TiAP (E_g ~3.25 eV) and P25 (E_g ~3.09 eV). A more detailed investigation of the other properties, including optical, morphological, structural, and photoelectrochemical characterization of TiAP and P25, is already discussed in our previous report [26].

3.2. Cytotoxicity assessment

Biological effects of TiAP and P25 on A549 pulmonary cells were investigated first. Analysis of the bacterial endotoxin presence in TiAP, P25, and multi-walled carbon nanotubes (MWCNT) showed no endotoxin levels (i.e., below the detection limit of the assay). Thus, the materials are considered endotoxin-free.

Cell viability was estimated by exploring the mitochondrial dehydrogenase activity using the WST-1 test (Table S1). Fig. 2A shows that TiAP and P25 significantly induced reduction of the dehydrogenase activity in A549 cells after 24 h and 48 h treatment, respectively. After 24 h (solid columns in Fig. 2A), the A549 cells treated with 100 μg.mL^{-1} of TiAP and P25 exhibited an insignificant decrease in cell viability. After 48 h (dashed columns in Fig. 2A), the reduction of the cell viability further decreased relatively to the increased concentrations. Indeed, 100 μg.mL^{-1} of TiAP and 100 μg.mL^{-1} of P25 induced the decrease of the cell viability to 85±3% ($p < 0.001$, vs. untreated cells) and 87±6% ($p < 0.001$, vs. untreated cells). According to the outcomes, a similar toxic effect of TiAP and P25 on dehydrogenase activity was determined. On the other hand, MWCNT treated cells exhibited the largest impairment after both 24 h (71±3%, $p < 0.001$, vs. untreated cells) and 48 h (77±4%, $p < 0.001$, vs. untreated cells).

Furthermore, the glutathione (GSH) levels in A549 cells were estimated via the bimane assay. The concentration-dependent results on the GSH levels in TiAP, P25, and MWCNT are summarized in Fig. 2B (Table S2). After 24 h (solid columns in Fig. 2B), the tested concentrations of TiAP significantly induced GSH depletion. In contrast, P25 induced significant GSH depletion only at the concentration of 100 μg.mL^{-1} after 24 h. After 48 h (dashed columns in Fig. 2B), the cells seemed to generally recover the GSH levels. Thus, a significant GSH depletion was present solely in the highest tested concentration (100 μg.mL^{-1}) of TiAP, and P25 treated cells. At this particular concentration, a decrease in GSH levels to 84±5% ($p < 0.001$, vs. untreated cells) and 91±5% ($p < 0.001$, vs. untreated cells) was observed in TiAP and P25, respectively. The largest cell impairment was observed in 100 μg.mL^{-1} MWCNT treated A549 cells, where the GSH levels decreased to approx. 60% in comparison to the untreated cells after both 24 h and 48 h.

Fluorescence microscopy imaging (Fig. 3) of pulmonary A549 cells after 24 h of incubation was undertaken to support the acquired quantitative data of the toxicity assessments (Fig. 2). Fluorescence staining of actin filaments (phalloidin-FITC probe, red color) and nuclei (Hoechst

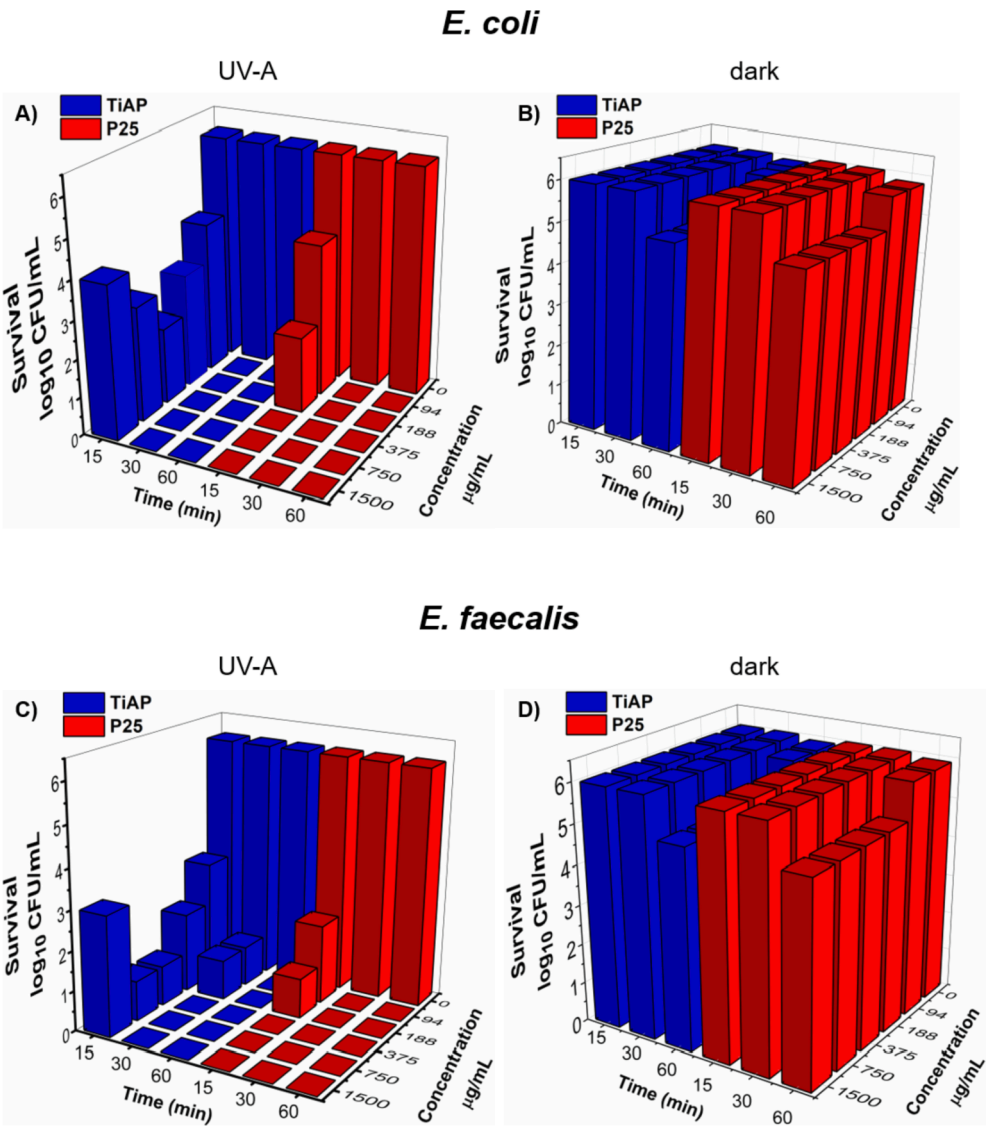

Fig. 5. Effect of TiAP and P25 on survival of planktonic cells of *E. faecalis* 37VRE and *E. coli* PA1 under UV-A (A,C) and in the dark (B,D), respectively. x-axis: time of exposure; y-axis: survival rate of bacteria; z-axis: concentration of TiAP and P25.

33258 dye, blue color) was used to define the functional morphology of A549 cells. Typical pebble-like morphology of A549 cells was documented. A comparable density (to control) of nuclei was observed in TiAP and P25 in concentrations 10 μg.mL^{-1} and 100 μg.mL^{-1}. However, a higher density of nuclei was determined in TiAP and P25 compared to that of MWCNT. These results are in good agreement with the obtained quantitative data in Fig. 2.

3.3. Photocatalytic activity

As second, the photocatalytic activity of TiAP and P25 was evaluated as the ability of the material to degrade model organic pollutants (i.e., methylene blue MB and caffeine CAF). The photocatalytic degradation of MB and CAF by TiO_2 nanopowders under solar-like irradiation is considered as a first-order kinetic reaction which is typical for TiO_2 photocatalysis [19]:

$$ln(c/c_0) = -kt \quad (1)$$

where c_0 is the initial concentration, c is the concentration at time t, and k is the apparent kinetic constant.

The calculated values of k for the different investigated photocatalytic systems are shown in Fig. 4. Repeated photocatalytic runs are shown in ESI (Fig. S4). In general, the differences between the repeated runs did not exceed ±5%, thus confirming the photocatalysts are stable and efficient over time. In pure water, higher degradation extents were obtained using TiAP for both MB (k = 0.265 min^{-1}) and CAF (k = 0.054 min^{-1}) compared to that of P25 (k = 0.214 min^{-1} for MB; k = 0.019 min^{-1} for CAF). The reasons behind these results are described by considering the specific surface area, morphology, and phase composition of TiO_2 nanopowders, which are important parameters for the material's photocatalytic performance [19,53]. Although the specific surface area of P25 (S_{BET} = 35.4 m^2.g^{-1}) is higher compared to TiAP (S_{BET} = 15.6 m^2.g^{-1}), P25 possessed a lower photocatalytic efficiency. Therefore, other parameters such as morphology (including the dimensionality) and phase composition of the material are predominant in the explanation of the overall photocatalytic efficiency. Here, TiAP is composed of 2D particles, whereas P25 is considered as 0D material. As already reported [54–56], a superior e^-/h^+ pairs separation and charge carrier transfer is present in 2D materials compared to 0D materials. In our previous work [26], a 10% increase in the incident-photon-to-electron conversion efficiency for TiAP compared to P25 was also observed. In other words, the amount of the photogenerated e^- and h^+ is increased within TiAP, thus leading to increased degradation of MB and

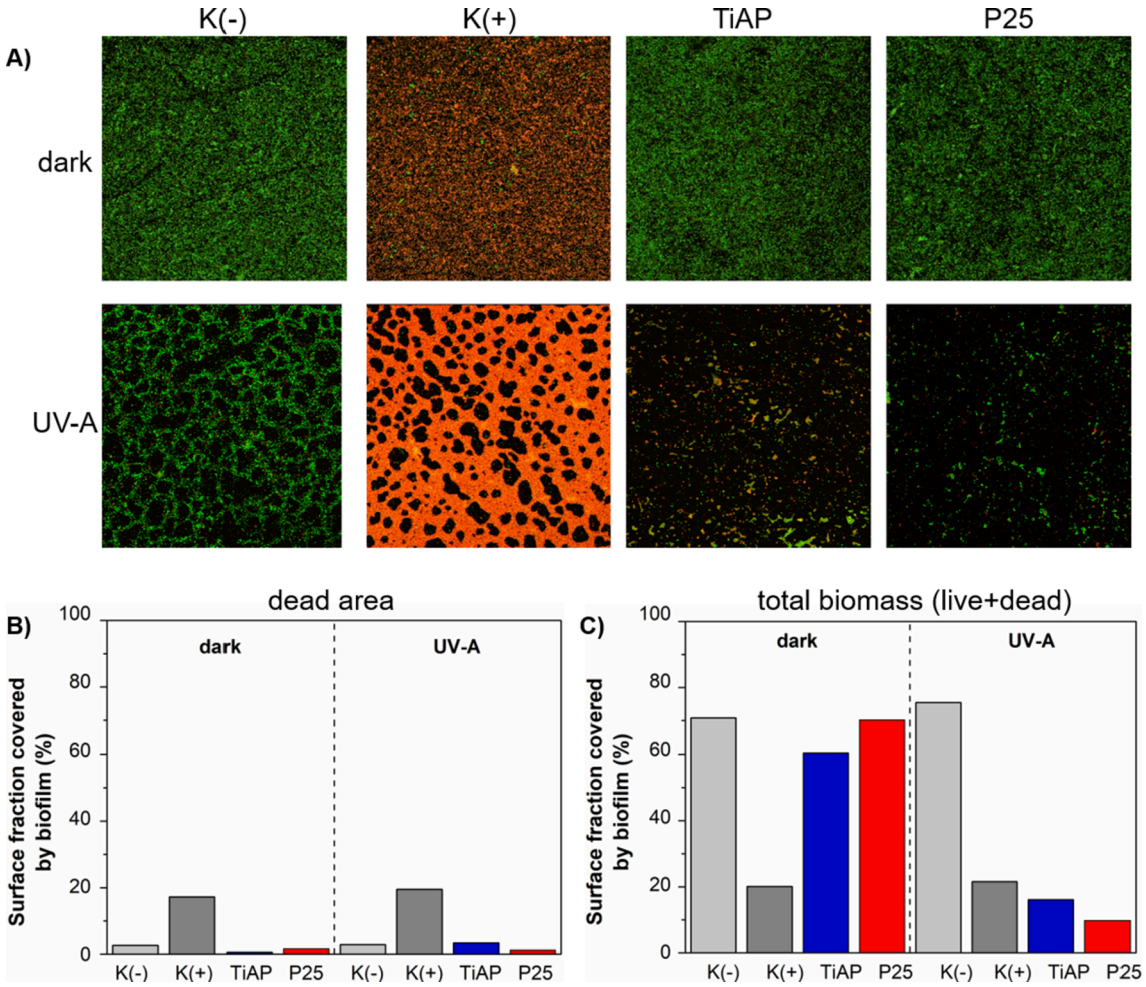

Fig. 6. *E. faecalis* killing percentage in biofilm condition analyzed by counting the live/dead bacteria. Comparison of antibiofilm effects of TiAP and P25 (188 μg.mL^{-1}); under UV-A and in the dark (60 min). A) Examples of confocal images showing the top view of 24 h developed biofilm formed by *E. faecalis* 37VRE. B) K(-) control live biofilm, and C) K(+) control dead biofilm (treated with 70% ethanol/10 min), biofilms treated with TiAP and P25 (188 μg.mL^{-1} for 60 min under UV-A/dark).

CAF. The suitable 2D morphology in TiAP offers an increased number of catalytic sites, while in P25, the particles are three-dimensionally connected, thus forming a nanoparticulate structure that does not offer a large amount of catalytic sites [57,58]. Moreover, there are multiple light scattering events that provide a higher number of photons that can be utilized in 2D materials. Concerning the role of the phase composition of TiO_2 for efficient photocatalysis, it still remains controversial. Indeed, anatase is more photoactive than rutile [59]. P25 predominantly contains anatase (approx. 80%) with approx. 20% of rutile, and it is considered as an optimal ratio for efficient photocatalysis [60], since at the interface anatase/rutile (at the heterojunction), the lifetime of e^-/h^+ pairs is enhanced due to beneficial charge carrier separation and transfer. On the other hand, TiAP consists solely of anatase TiO_2. In the present work, considering all these various aspects, the interplay of the specific surface area, morphology, and phase composition are undoubtedly important factors but it appears that the morphology is the predominant one since TiAP is more efficient than P25 for the photocatalytic degradation of MB and CAF.

In physiological solution, photocatalytic efficiency of TiAP (TiAP-ph, $k = 0.109\ min^{-1}$ for MB; $k = 0.022\ min^{-1}$ for CAF) was also higher than that of P25 (P25-ph, $k = 0.115\ min^{-1}$ for MB; $k = 0.013\ min^{-1}$ for CAF). However, compared to a pure water system, the degradation extents in physiological solutions were lower. That is due to the presence of chloride ions which limit the action of hydroxyl radicals according to the reactions (Eq. (2) and (3)).

$$Cl^- + HO\bullet \rightarrow HOCl\bullet^- \quad (2)$$

$$HOCl\bullet^- + Cl^- \rightarrow Cl_2\bullet^- + OH^- \quad (3)$$

Other inhibition mechanisms can be involved, such as 1) blocking of the active surface sites by chloride adsorption [61–67] and 2) increasing aggregation of TiO_2 particles [68]. Nevertheless, approx. 70 % of MB and > 30% of CAF was degraded using both TiAP and P25 after 10 and 30 min, respectively.

To demonstrate the photocatalytic activity of TiAP and P25, HO• were analyzed by fluorescence spectroscopy since they are considered as the main ROS in the degradation of organic pollutants such as MB and CAF. The generation of HO• under solar-like irradiation over time is summarized in Fig. 4C. The data support the resulting photocatalytic measurements since the highest production rate of hydroxyl-terephthalic acid is obtained for TiAP (approx. 1.1×10^{-6} mol.L^{-1}) followed by P25, TiAP-ph, and P25-ph (between 7×10^{-7} mol.L^{-1} – 8×10^{-7} mol.L^{-1}) after 10 min.

From these photocatalytic results, it is clear that TiAP is a better photocatalyst than P25 in a pure water system. However, in physiological solution, both nanopowders have similar efficiency, thus highlighting that TiAP is more susceptible to the chemical environment than P25.

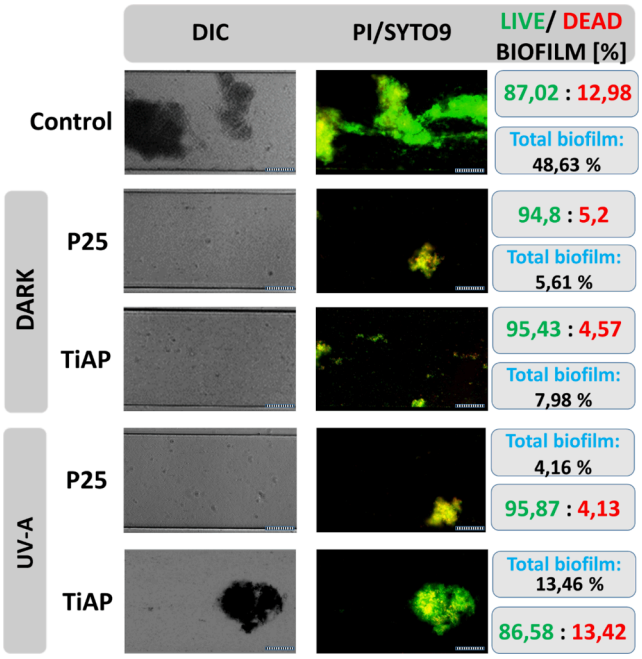

Fig. 7. Imaging of the channel cross-section with *E. faecalis* biofilms after 24 h of incubation at flow conditions (0.5 dyn.cm^{-2}). Biofilms were formed by bacteria treated with TiAP and P25 (188 μg.mL^{-1}) under 60 min of UV-A and in the dark. Left column images – biofilms visualized using differential interference contrast (DIC); right column images – biofilms stained with Syto9 (live cells; green fluorescence) and PI (dead cells; red fluorescence). Control – untreated bacteria; scale bar = 100 μm.

3.4. Photoinduced antimicrobial and antibiofilm performance

At last, photoinduced antimicrobial and antibiofilm activity of TiAP and P25 against planktonic (free living) and biofilm (sessile) forms of bacteria was evaluated in the dark and under UV-A light at different concentrations (94 μg.mL^{-1}, 188 μg.mL^{-1}, 375 μg.mL^{-1}, 750 μg.mL^{-1}, and 1500 μg.mL^{-1}). Fig. 5 shows the survival rate (ability to grow) of planktonic *E. coli* (Gram-negative) and *E. faecalis* (Gram-positive). In the dark and under UV-A without TiAP and P25 (Fig. 5), no significant antibacterial effect was detected (6 log$_{10}$ CFU.mL^{-1} after 60 min exposure). However, after 60 min exposure to TiAP and P25 in the dark, a small reduction of bacteria (~5 log$_{10}$ CFU.mL^{-1}) was present. Indeed, the fragmentation (by mechanical force of the nanoparticles) of the *E. coli* and *E. faecalis* cell membrane by TiAP and P25 is responsible for such a result [21,22]. This mechanism is described as following. Interaction between TiAP/P25 with the bacterial membrane induces an increase in the membrane tension due to the adsorbed nanoparticles of TiAP/P25 to the cell membrane [22] that result to the cell fragmentation and subsequently to cell death. After UV-A irradiation for 15 min, 30 min, and 60 min in the presence of TiAP and P25, the survival rate of bacteria decreased significantly, as illustrated in Fig. 5A (*E. coli*) and Fig. 5C (*E. faecalis*). After 60 min, a complete 6 log$_{10}$ CFU.mL^{-1} reduction of both bacteria was obtained for all concentrations of TiAP and P25, respectively. However, as nanopowders concentration decreases and irradiation time is shortened, the photo-induced antimicrobial efficiency decreases, especially for TiAP. Indeed, after 15 min, for P25, a survival of *E. coli* (4 log$_{10}$ CFU.mL^{-1} and 2 log$_{10}$ CFU.mL^{-1}) and *E. faecalis* (2 log$_{10}$ CFU.mL^{-1} and 1 log$_{10}$ CFU.mL^{-1}) was obtained for concentrations of 94 μg.mL^{-1} and 188 μg.mL^{-1}, respectively, while in the presence of TiAP, both the bacteria still survived whatever the concentration of TiAP. Interestingly, at the highest concentration of TiAP (1500 μg.mL^{-1}), an increase in the survival rate of bacteria was present. That can reflect the dosage-dependent antibacterial effect, where the amount of killed bacteria was strongly dependent on the formation of nanoparticle aggregates. Indeed, TiAP is prone to form larger agglomerates compared to P25. The dense clusters of nanoparticles blocked the access of ROS to the bacterial cells. This phenomenon was observed after a short exposure time (15 min), while longer UV-A irradiation abolished this effect. A similar phenomenon was previously reported [69,70].

The photoinduced inactivation of planktonic cells showed no significant resistance to ROS. Nevertheless, the penetration of the biofilm by the oxidizing agents might be challenging. Therefore, the study of TiAP and P25 against a) the already formed biofilm and b) in preventing the biofilm formation was conducted (Fig. 6). In these studies, a relatively low concentration of TiAP and P25 (188 μg.mL^{-1}) was used, so a significant but not 100% reduction of bacteria was demonstrated. Indeed, keeping part of the population alive is essential for biofilm production. Moreover, as described above, a lower concentration of TiAP and P25 prevents the formation of large agglomerates that limits their antimicrobial activity. Therefore, to evaluate TiAP and P25 antibiofilm performance against mature biofilms, 24 h *E. faecalis* biofilm was uniformly formed across a glass substrate under static conditions. To note, *E. coli* did not produce biofilms under the used experimental conditions; therefore, they were not further studied. Confocal Laser Scanning Microscopy (CLSM) show the total biomass of *E. faecalis* (live and dead cells) exposed to TiAP and P25 along with the negative K(-) and positive K(+) control in the dark and under UV-A (Fig. 6A). The total biomass for TiAP and P25 treated biofilms decreased from 60.5% (dark) to 16% (UV-A) and from 70% (dark) to 10% (UV-A), respectively (Fig. 6C). Fig. 6B shows a quantitative analysis of the proportion of dead cells in the biofilms. After 60 min UV-A irradiation, the percentage of dead cells in the biofilms was following: 4% (untreated cells), 91% (control biofilm treated with ethanol), 21% (biofilm treated with TiAP), and 15% (biofilm treated with P25). The antibiofilm performance of TiAP and P25 was lower compared to that of the planktonic forms of *E. faecalis*. Indeed, the biofilm cells exhibit higher tolerance to most microbial agents compared to that of the planktonic ones. The crucial feature that clearly distinguishes biofilms from their planktonic counterparts is conditioned by the production of a protective extracellular matrix (ECM), the presence of a specialized persister cells, and an ability to coordinate the metabolic functions of all biofilm cells (quorum sensing phenomenon) [71]. Considering the relatively low concentration of TiAP and P25, a considerable high antibiofilm performance was achieved.

To obtain a deeper understanding of the antibiofilm performance of TiAP and P25, biofilm formation in microfluidic conditions was also evaluated. Fig. 7 shows the visual presentation (channels of BioFlux plate) of 24 h *E. faecalis* biofilms. They were developed after 60 min exposure of the cells to TiAP and P25 with the concentration of 188 μg.mL^{-1} in the dark and under UV-A light. The total control surface (not treated with TiAP and P25) area covered by the biofilm was approx. 48.63% with the biofilm viability of 87.02 %. After exposing the cells to TiAP and P25, a substantial decrease of the adhesion process, thus limiting the biofilm formation, was observed. In the dark, approx. 7.98% and 5.61% surface area was covered by the biofilm after exposure to TiAP and P25, respectively. After 60 min UV-A irradiation, a further decrease in the biofilm formation was obtained only for P25 (covered surface area approx. 4.16%). In the case of TiAP, approx. 13% of the surface area was covered by the biofilm. These differences are due to the tendency of TiAP to form more aggregates than P25 and the formation of bacterial aggregates with TiAP nanoparticles under UV-A. In the long run, such structures are a source of oxidative stress, deadly for bacteria [72]. Overall, a strong impact of TiAP and P25 on the viability, adhesion, and ability to produce biofilm by *E. faecalis*, under flow conditions was determined.

To get better insights into antimicrobial and antibiofilm mechanism, levels of the intracellular reactive oxygen species (iROS) was evaluated via CellROX Green and DHE probes. In vitro, the CellROX dye is oxidized exclusively by intracellular superoxide ($O_2^{\bullet-}$) and by hydroxyl radical

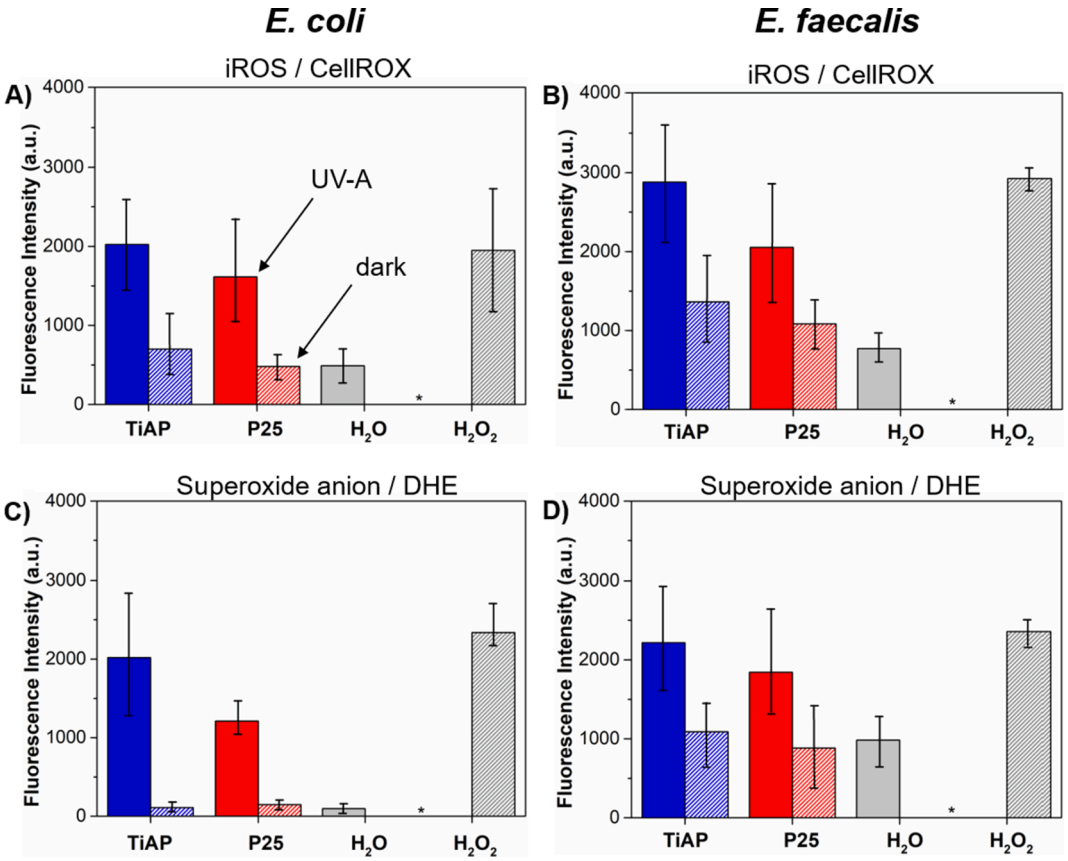

Fig. 8. Intracellular oxidative stress generated within cells of E. *faecalis* 37VRE and *E.coli* PA1 treated by TiAP and P25, water and hydrogen peroxide (1.5% H_2O_2), in the presence or absence of UV-A for 60 min. A,B) intracellular ROS measured by CellROX^{TM} Green Reagent, C,D) intracellular superoxide anion (O_2•-) measured by the dihydroethidium (DHE) probe. The absolute fluorescence value was corrected by subtracting the fluorescence value for a sample in water with the absence of UV-A. (*) - indicates zero (corrected fluorescence value).

(HO•). However, the probe cannot differentiate the ROS subspecies. With the DHE probe, only total cellular O_2•$^-$ production can be detected [73]. Besides the fragmentation of the cell membrane, the mechanism that led to the photoinduced inactivation of *E. faecalis* and *E. coli* by TiAP and P25 primarily depends on the amount of the produced iROS. An increase in iROS levels resulted in a collapse of the cellular antioxidant defense that subsequently led to oxidative stress. This state resulted in intracellular compounds damage and cell death [74]. Fig. 8A and C shows the produced amount of HO• and O_2•$^-$ (iROS) as the dependency of the fluorescence levels after 60 min UV-A irradiation and in the dark (bacteria exposed to 1.5% H_2O_2 for 60 min in the dark was used as a positive control). A strong response was observed for TiAP and P25 at the concentration of 188 μg.mL^{-1}. In general, a higher concentration of iROS was produced in TiAP than in P25 under UV-A light and in the dark. Thus, higher oxidative stress was generated by TiAP in both types of bacteria (Fig. 8A and B). The levels of O_2•$^-$ in TiAP and P25 are shown in Fig. 8C and D. For TiAP, a higher concentration of O_2•$^-$ was generated than in P25. The overall oxidative stress for *E. coli* was lower compared to *E. faecalis*. The exact mechanism of the photocatalytic inactivation of bacteria is not fully understood yet. However, it is presumed to be largely dependent on the chemical structure and overall complexity of the cellular sheaths [74]. Overall, it is accepted that the oxidizing agents first attack the bacterial cell walls, which is different in Gram-negative *E. coli* than in Gram-positive *E. faecalis* [75]. A Gram-negative cell wall is more complex due to an additional outer membrane consisted of a two lipid barrier [76]. Thus the outer membrane act as a natural barrier for the generated ROS and selectively blocks the particles transfer into the cell interior.

4. Conclusions

TiO_2 aerogel powders prepared by lyophilization and commercially available TiO_2 P25 are critically compared for cytotoxicity, photocatalytic activity, antibacterial, and antibiofilm performance. Both nanopowders showed different photocatalytic and biological properties due to their crystallite size, phase, shape, morphology, and surface area, i.e., TiAP possess a 2D and P25 a 0D morphology. Cytotoxicity assessment of A549 pulmonary cells by measuring the dehydrogenase activity and glutathione levels showed a low level of toxicity for both TiAP and P25. TiAP showed better photocatalytic activity under UV-A irradiation in the degradation of methylene blue and caffeine in pure water and physiological solution than P25 due to more catalytic sites of TiAP, which in turn produces more HO$^{\bullet}$ radicals for the photodegradation of the pollutants. However, the photodegradation of the pollutants in physiological solution exhibited a lower degradation extent for both TiAP and P25 than the pure water since Cl^- ions act as a scavenger of HO$^{\bullet}$ radicals. The antimicrobial studies on planktonic *E. coli* and *E. faecalis* for both TiAP and P25 under UV-A irradiation for 60 min showed complete inactivation of the bacteria from 6 $\log_{10}$ CFU.mL^{-1} to zero for all concentrations of the nanopowders. Interestingly, lower concentration and shorter UV-A irradiation time of 15 min showed insufficient inactivation of the bacteria by the nanopowders, especially TiAP was less efficient than P25. Moreover, the antibiofilm performance of TiAP and P25 under UV-A irradiation studied using *E. faecalis* was similar. The effect of oxidative stress by TiO_2 nanopowders is different according to the complexity of the bacterial cell wall, wherein *E. faecalis* showed higher oxidative stress than *E. coli*. Thus, the cytotoxicity, photocatalytic, antibacterial, and antibiofilm experiments showed the

benefits and drawbacks of TiAP and P25 under different experimental conditions, thereby opening a pathway to use these nanopowders efficiently for environmental and biological applications. Indeed, regarding the results of this critical comparison between P25 and TiAP, it appears that although P25 is, so far, economically more advantegeous than the newly designed 2D TiO_2 nanopowders, these 2D TiO_2 nanopowders appear promising mainly in term of photocatalytic efficiency.

CRediT authorship contribution statement

Guru Karthikeyan Thirunavukkarasu: Investigation, Visualization. **Jana Bacova:** Investigation, Writing – review & editing, Methodology. **Olivier Monfort:** Writing – review & editing, Investigation, Visualization. **Ewa Dworniczek:** Writing – review & editing, Methodology, Resources. **Emil Paluch:** Visualization, Methodology, Investigation. **Muhammad Bilal Hanif:** Visualization, Methodology. **Sajid Rauf:** Methodology. **Monika Motlochova:** Methodology. **Jan Capek:** Methodology. **Karol Hensel:** Investigation, Writing – review & editing, Resources. **Gustav Plesch:** Writing – review & editing, Visualization. **Grzegorz Chodaczek:** Investigation. **Tomas Rousar:** Writing – review & editing, Methodology, Investigation, Resources. **Martin Motola:** Supervision, Conceptualization, Writing – review & editing, Visualization.

Declaration of Competing Interest

The authors declare that they have no known competing financial interests or personal relationships that could have appeared to influence the work reported in this paper.

Acknowledgements

Authors acknowledge the financial support provided by the Scientific Grant Agency of the Slovak Republic (project VEGA 1/0712/18) and the Slovak Research and Development Agency (projects APVV-17-0324, APVV-20-0566). This work was also funded by the Wroclaw Medical University (statutory research SUB.A. 130.21.031). The financial support was received from the Ministry of Education, Youth and Sports of the Czech Republic via project NANOBIO (Reg. No. CZ.02.1.01/0.0/0.0/17_048/0007421). We thank Jan Subrt, Alicja Seniuk and Aleksandra Lavrikova for help with running the experiments.

Appendix A. Supplementary material

Supplementary data to this article can be found online at https://doi.org/10.1016/j.apsusc.2021.152145.

References

[1] C. Renz, Lichtreaktionen der oxyde des titans, cers und der erdsäuren, Helv. Chim. Acta. 4 (1) (1921) 961–968, https://doi.org/10.1002/hlca.192100401101.
[2] A.E. Jacobsen, Titanium dioxide pigments: correlation between photochemical reactivity and chalking, Ind. Eng. Chem. 41 (3) (1949) 523–526, https://doi.org/10.1021/ie50471a018.
[3] A. Fujishima, K. Honda, Electrochemical photolysis of water at a semiconductor electrode, Nature. 238 (5358) (1972) 37–38, https://doi.org/10.1038/238037a0.
[4] J.H. Carey, J. Lawrence, H.M. Tosine, Photodechlorination of PCB's in the presence of titanium dioxide in aqueous suspensions, Bull. Environ. Contam. Toxicol. 16 (6) (1976) 697–701, https://doi.org/10.1007/BF01685575.
[5] S.N. Frank, A.J. Bard, Heterogeneous photocatalytic oxidation of cyanide ion in aqueous solutions at TiO_2 powder, J. Am. Chem. Soc. 99 (1977) 303–304, https://doi.org/10.1021/ja00443a081.
[6] T. Matsunaga, R. Tomoda, T. Nakajima, H. Wake, Photoelectrochemical sterilization of microbial cells by semiconductor powders, FEMS Microbiol. Lett. 29 (1985) 211–214, https://doi.org/10.1111/j.1574-6968.1985.tb00864.x.
[7] J.C. Sjogren, R.A. Sierka, Inactivation of phage MS_2 by iron-aided titanium dioxide photocatalysis, Appl. Environ. Microbiol. 60 (1) (1994) 344–347, https://doi.org/10.1128/aem.60.1.344-347.1994.
[8] A.-G. Rincón, C. Pulgarin, Bactericidal action of illuminated TiO_2 on pure Escherichia coli and natural bacterial consortia: Post-irradiation events in the dark and assessment of the effective disinfection time, Appl. Catal. B Environ. 49 (2) (2004) 99–112, https://doi.org/10.1016/j.apcatb.2003.11.013.
[9] F. Shiraishi, K. Toyoda, S. Fukinbara, E. Obuchi, K. Nakano, Photolytic and photocatalytic treatment of an aqueous solution containing microbial cells and organic compounds in an annular-flow reactor, Chem. Eng. Sci. 54 (10) (1999) 1547–1552, https://doi.org/10.1016/S0009-2509(99)00068-8.
[10] W.A. Jacoby, P.C. Maness, E.J. Wolfrum, D.M. Blake, J.A. Fennell, Mineralization of bacterial cell mass on a photocatalytic surface in air, Environ. Sci. Technol. 32 (17) (1998) 2650–2653, https://doi.org/10.1021/es980036f.
[11] D.M. Blake, P.-C. Maness, Z. Huang, E.J. Wolfrum, J. Huang, W.A. Jacoby, Application of the photocatalytic chemistry of titanium dioxide to disinfection and the killing of cancer cells, Sep. Purif. Methods. 28 (1) (1999) 1–50, https://doi.org/10.1080/03602549909351643.
[12] C. Wei, W.Y. Lin, Z. Zainal, N.E. Williams, K. Zhu, A.P. Kruzic, R.L. Smith, K. Rajeshwar, Bactericidal activity of TiO_2 photocatalyst in aqueous media: toward a solar-assisted water disinfection system, Environ. Sci. Technol. 28 (5) (1994) 934–938, https://doi.org/10.1021/es00054a027.
[13] M.V. Selma, A. Allende, F. López-Gálvez, M.Á. Conesa, M.I. Gil, Heterogeneous photocatalytic disinfection of wash waters from the fresh-cut vegetable industry, J. Food Prot. 71 (2008) 286–292, https://doi.org/10.4315/0362-028X-71.2.286.
[14] J. Araña, J.A. Herrera Melián, J.M. Doña Rodríguez, O. González Díaz, A. Viera, J. Pérez Peña, P.M. Marrero Sosa, V. Espino Jiménez, TiO_2-photocatalysis as a tertiary treatment of naturally treated wastewater, Catal. Today 76 (2-4) (2002) 279–289, https://doi.org/10.1016/S0920-5861(02)00226-2.
[15] B. Rong Wang, K. Hashimoto, A. Fujishima, M. Chikuni, E. Kojima, A. Kitamura, M. Shimohigoshi, T. Watanabe, A. Fujishima, R. Wang, K. Hashimoto, T. Watanabe, M. Chikuni, E. Kojima, A. Kitamura, M. Shimohigoshi, Photogeneration of Highly Amphiphilic TiO_2 Surfaces, 1998. https://doi.org/10.1002/(SICI)1521-4095(199801)10:2.
[16] R. Wang, K. Hashimoto, A. Fujishima, M. Chikuni, E. Kojima, A. Kitamura, M. Shimohigoshi, T. Watanabe, Light-induced amphiphilic surfaces, Nature 388 (6641) (1997) 431–432, https://doi.org/10.1038/41233.
[17] D.Y. Goswami, D.M. Trivedp, S.S. Block, Photocatalytic disinfection of indoor air, J. Sol. Energy Eng. Trans. ASME. 119 (1997) 92–96, https://doi.org/10.1115/1.2871871.
[18] Y. Kikuchi, K. Sunada, T. Iyoda, K. Hashimoto, A. Fujishima, Photocatalytic bactericidal effect of TiO_2 thin films: dynamic view of the active oxygen species responsible for the effect, J. Photochem. Photobiol. A Chem. 106 (1-3) (1997) 51–56, https://doi.org/10.1016/S1010-6030(97)00038-5.
[19] J. Schneider, M. Matsuoka, M. Takeuchi, J. Zhang, Y.u. Horiuchi, M. Anpo, D. W. Bahnemann, Understanding TiO_2 photocatalysis: mechanisms and materials, Chem. Rev. 114 (19) (2014) 9919–9986, https://doi.org/10.1021/cr5001892.
[20] S.P. Albu, A. Ghicov, S. Aldabergenova, P. Drechsel, D. LeClere, G.E. Thompson, J. M. Macak, P. Schmuki, Formation of double-walled TiO2 nanotubes and robust anatase membranes, Adv. Mater. (2008) NA–NA, https://doi.org/10.1002/adma.200801189.
[21] H.-M. Ding, Y.-Q. Ma, Computational approaches to cell-nanomaterial interactions: keeping balance between therapeutic efficiency and cytotoxicity, Nanoscale Horizons. 3 (1) (2018) 6–27.
[22] D.P. Linklater, V.A. Baulin, X. Le Guével, J.-B. Fleury, E. Hanssen, T.H.P. Nguyen, S. Juodkazis, G. Bryant, R.J. Crawford, P. Stoodley, E.P. Ivanova, Antibacterial action of nanoparticles by lethal stretching of bacterial cell membranes, Adv. Mater. 32 (52) (2020) 2005679, https://doi.org/10.1002/adma.v32.5210.1002/adma.202005679.
[23] K. Hashimoto, H. Irie, A. Fujishima, TiO_2 photocatalysis: a historical overview and future prospects, Japanese J. Appl. Physics, Part 1 Regul. Pap. Short Notes Rev. Pap. 44 (12) (2005) 8269–8285, https://doi.org/10.1143/JJAP.44.8269.
[24] S.G. Kumar, L.G. Devi, Review on modified TiO_2 photocatalysis under UV/visible light: selected results and related mechanisms on interfacial charge carrier transfer dynamics, J. Phys. Chem. A. 115 (46) (2011) 13211–13241, https://doi.org/10.1021/jp204364a.
[25] M. Motola, R. Zazpe, L. Hromadko, J. Prikryl, V. Cicmancova, J. Rodriguez-Pereira, H. Sopha, J.M. Macak, Anodic TiO_2 nanotube walls reconstructed: inner wall replaced by ALD TiO_2 coating, Appl. Surf. Sci. 549 (2021) 149306, https://doi.org/10.1016/j.apsusc.2021.149306.
[26] G.K. Thirunavukkarasu, O. Monfort, M. Motola, M. Motlochová, M. Gregor, T. Roch, M. Čaplovicová, A.Y. Lavrikova, K. Hensel, V. Brezová, M. Jerigová, J. Šubrt, G. Plesch, Ce ion surface-modified TiO_2 aerogel powders: a comprehensive study of their excellent photocatalytic efficiency in organic pollutant removal, New J. Chem. 45 (9) (2021) 4174–4184.
[27] V.K. Yemmireddy, Y.-C. Hung, Using photocatalyst metal oxides as antimicrobial surface coatings to ensure food safety—opportunities and challenges, Compr. Rev. Food Sci. Food Saf. 16 (4) (2017) 617–631, https://doi.org/10.1111/1541-4337.12267.
[28] U. Joost, K. Juganson, M. Visnapuu, M. Mortimer, A. Kahru, E. Nõmmiste, U. Joost, V. Kisand, A. Ivask, Photocatalytic antibacterial activity of nano-TiO_2 (anatase)-based thin films: effects on Escherichia coli cells and fatty acids, J. Photochem. Photobiol. B Biol. 142 (2015) 178–185, https://doi.org/10.1016/j.jphotobiol.2014.12.010.
[29] A. Kubacka, M.S. Diez, D. Rojo, R. Bargiela, S. Ciordia, I. Zapico, J.P. Albar, C. Barbas, V.A.P. Martins Dos Santos, M. Fernández-García, M. Ferrer, Understanding the antimicrobial mechanism of TiO_2-based nanocomposite films in a pathogenic bacterium, Sci. Rep. 4 (2014) 1–9, https://doi.org/10.1038/srep04134.
[30] R. Fagan, D.E. McCormack, D.D. Dionysiou, S.C. Pillai, A review of solar and visible light active TiO_2 photocatalysis for treating bacteria, cyanotoxins and contaminants of emerging concern, Mater. Sci. Semicond. Process. 42 (2016) 2–14, https://doi.org/10.1016/j.mssp.2015.07.052.

[31] M. Motola, E. Dworniczek, L. Satrapinskyy, G. Chodaczek, J. Grzesiak, M. Gregor, T. Plecenik, J. Nowicka, G. Plesch, UV light-induced photocatalytic, antimicrobial, and antibiofilm performance of anodic TiO_2 nanotube layers prepared on titanium mesh and Ti sputtered on silicon, Chem. Pap. 73 (5) (2019) 1163–1172, https://doi.org/10.1007/s11696-018-0667-4.

[32] H.M.K.K. Pathirana, R.A. Maithreepala, Photodegradation of 3,4-dichloropropionamide in aqueous TiO_2 suspensions, J. Photochem. Photobiol. A Chem. 102 (2-3) (1997) 273–277, https://doi.org/10.1016/S1010-6030(96)04455-3.

[33] V. Augugliaro, V. Loddo, G. Marcì, L. Palmisano, M.J. López-Muñoz, Photocatalytic oxidation of cyanides in aqueous titanium dioxide suspensions, J. Catal. 166 (2) (1997) 272–283, https://doi.org/10.1006/jcat.1997.1496.

[34] T.Y. Wei, C.C. Wan, Heterogeneous photocatalytic oxidation of phenol with titanium dioxide powders, Ind. Eng. Chem. Res. 30 (6) (1991) 1293–1300, https://doi.org/10.1021/ie00054a033.

[35] V. Štengl, S. Bakardjieva, J. Šubrt, L. Szatmary, Titania aerogel prepared by low temperature supercritical drying, Microporous Mesoporous Mater. 91 (1-3) (2006) 1–6, https://doi.org/10.1016/j.micromeso.2005.10.046.

[36] O. Carp, C.L. Huisman, A. Reller, Photoinduced reactivity of titanium dioxide, Prog. Solid State Chem. 32 (2004) 33–177, https://doi.org/10.1016/j.progsolidstchem.2004.08.001.

[37] X. Jiang, M. Manawan, T. Feng, R. Qian, T. Zhao, G. Zhou, F. Kong, Q. Wang, S. Dai, J.H. Pan, Anatase and rutile in evonik aeroxide P25: Heterojunctioned or individual nanoparticles? Catal. Today 300 (2018) 12–17, https://doi.org/10.1016/j.cattod.2017.06.010.

[38] R. Koirala, S.E. Pratsinis, A. Baiker, Synthesis of catalytic materials in flames: opportunities and challenges, Chem. Soc. Rev. 45 (11) (2016) 3053–3068.

[39] B. Ohtani, Preparing articles on photocatalysis - beyond the illusions, misconceptions, and speculation, Chem. Lett. 37 (3) (2008) 216–229, https://doi.org/10.1246/cl.2008.216.

[40] D. Friedmann, A. Hakki, H. Kim, W. Choi, D. Bahnemann, Heterogeneous photocatalytic organic synthesis: state-of-the-art and future perspectives, Green Chem. 18 (20) (2016) 5391–5411.

[41] J. Zhao, Y. He, L. Zhang, K. Lu, Preparation of porous TiO_2 powder with mesoporous structure by freeze-drying method, J. Alloys Compd. 678 (2016) 36–41, https://doi.org/10.1016/j.jallcom.2016.03.253.

[42] S. Vafaei, L. Splingaire, U. Schnupf, K. Hisae, D. Hasegawa, T. Sugiura, K. Manseki, Low temperature synthesis of anatase TiO_2 nanocrystals using an organic-inorganic gel precursor, Powder Technol. 368 (2020) 237–244, https://doi.org/10.1016/j.powtec.2020.04.060.

[43] J. Šubrt, P. Pulišová, J. Boháček, P. Bezdička, E. Pližingrová, L. Volfová, J. Kupčík, Highly photoactive 2D titanium dioxide nanostructures prepared from lyophilized aqueous colloids of peroxo-polytitanic acid, Mater. Res. Bull. 49 (2014) 405–412, https://doi.org/10.1016/j.materresbull.2013.09.028.

[44] C.O. Robichaud, A.E. Uyar, M.R. Darby, L.G. Zucker, M.R. Wiesner, Estimates of upper bounds and trends in nano-TiO_2 production as a basis for exposure assessment, Environ. Sci. Technol. 43 (12) (2009) 4227–4233, https://doi.org/10.1021/es8032549.

[45] E. Pližingrová, L. Volfová, P. Svora, N.K. Labhsetwar, M. Klementová, L. Szatmáry, J. Šubrt, Highly photoactive anatase foams prepared from lyophilized aqueous colloids of peroxo-polytitanic acid, Catal. Today 240 (2015) 107–113, https://doi.org/10.1016/j.cattod.2014.04.022.

[46] S. Brunauer, P.H. Emmett, E. Teller, Adsorption of Gases in Multimolecular Layers, J. Am. Chem. Soc. 60 (2) (1938) 309–319, https://doi.org/10.1021/ja01269a023.

[47] J. Čapek, M. Hauschke, L. Brůčková, T. Roušar, Comparison of glutathione levels measured using optimized monochlorobimane assay with those from ortho-phthalaldehyde assay in intact cells, J. Pharmacol. Toxicol. Methods 88 (2017) 40–45, https://doi.org/10.1016/j.vascn.2017.06.001.

[48] R. Michal, E. Dworniczek, M. Čaplovičová, M. Gregor, L. Čaplovič, A. Seniuk, P. Kuš, G. Plesch, Photocatalytic and photodisinfectant activity of sulfated and Eu doped anatase against clinically important microorganisms, Ceram. Int. 40 (4) (2014) 5745–5756, https://doi.org/10.1016/j.ceramint.2013.11.013.

[49] N.D. Thorat, E. Dworniczek, G. Brennan, G. Chodaczek, R. Mouras, V. Gascón Pérez, C. Silien, S.A.M. Tofail, J. Bauer, Photo-responsive functional gold nanocapsules for inactivation of community-acquired, highly virulent, multidrug-resistant MRSA, J. Mater. Chem. B 9 (3) (2021) 846–856, https://doi.org/10.1039/d0tb02047h.

[50] E. Kolderman, D. Bettampadi, D. Samarian, S.E. Dowd, B. Foxman, N. S. Jakubovics, A.H. Rickard, A. Al-Ahmad, L-arginine destabilizes oral multi-species biofilm communities developed in human saliva, PLoS One. 10 (5) (2015) e0121835, https://doi.org/10.1371/journal.pone.0121835.

[51] Q. Wang, E.F. De Oliveira, S. Alborzi, L.J. Bastarrachea, R.V. Tikekar, On mechanism behind UV-A light enhanced antibacterial activity of gallic acid and propyl gallate against Escherichia coli O157:H7, Sci. Rep. 7 (2017) 1–11, https://doi.org/10.1038/s41598-017-08449-1.

[52] E. Pližingrová, M. Klementová, P. Bezdička, J. Boháček, Z. Barbieriková, D. Dvoranová, M. Mazúr, J. Krýsa, J. Šubrt, V. Brezová, 2D-Titanium dioxide nanosheets modified with Nd, Ag and Au: preparation, characterization and photocatalytic activity, Catal. Today 281 (2017) 165–180, https://doi.org/10.1016/J.CATTOD.2016.08.013.

[53] A.L. Linsebigler, G. Lu, J.T. Yates, Photocatalysis on TiO_2 surfaces: principles, mechanisms, and selected results, Chem. Rev. 95 (3) (1995) 735–758, https://doi.org/10.1021/cr00035a013.

[54] L. Sheng, T. Liao, L. Kou, Z. Sun, Single-crystalline ultrathin 2D TiO_2 nanosheets: a bridge towards superior photovoltaic devices, Mater. Today Energy 3 (2017) 32–39, https://doi.org/10.1016/j.mtener.2016.12.004.

[55] M. Velický, P.S. Toth, From two-dimensional materials to their heterostructures: an electrochemist's perspective, Appl. Mater. Today. 8 (2017) 68–103, https://doi.org/10.1016/j.apmt.2017.05.003.

[56] S.H. Mir, V.K. Yadav, J.K. Singh, J.K. Singh, Recent advances in the carrier mobility of two-dimensional materials: a theoretical perspective, ACS Omega 5 (2020) 14203–14211, https://doi.org/10.1021/acsomega.0c01676.

[57] B. Luo, G. Liu, L. Wang, Recent advances in 2D materials for photocatalysis, Nanoscale 8 (13) (2016) 6904–6920.

[58] S. Nakade, Y. Saito, W. Kubo, T. Kitamura, Y. Wada, S. Yanagida, Influence of TiO_2 nanoparticle size on electron diffusion and recombination in dye-sensitized TiO_2 solar cells, J. Phys. Chem. B 107 (33) (2003) 8607–8611, https://doi.org/10.1021/jp034773w.

[59] T. Luttrell, S. Halpegamage, J. Tao, A. Kramer, E. Sutter, M. Batzill, Why is anatase a better photocatalyst than rutile? - model studies on epitaxial TiO_2 films, Sci. Rep. 4 (2015) 1–8, https://doi.org/10.1038/srep04043.

[60] R.I. Bickley, T. Gonzalez-Carreno, J.S. Lees, L. Palmisano, R.J.D. Tilley, A structural investigation of titanium dioxide photocatalysts, J. Solid State Chem. 92 (1) (1991) 178–190, https://doi.org/10.1016/0022-4596(91)90255-G.

[61] M. Krivec, R. Dillert, D.W. Bahnemann, A. Mehle, J. Štrancar, G. Dražić, The nature of chlorine-inhibition of photocatalytic degradation of dichloroacetic acid in a TiO_2-based microreactor, in, Phys. Chem. Chem. Phys., Royal Soc. Chem. (2014) 14867–14873, https://doi.org/10.1039/c4cp01043d.

[62] H.Y. Chen, O. Zahraa, M. Bouchy, Inhibition of the adsorption and photocatalytic degradation of an organic contaminant in an aqueous suspension of TiO_2 by inorganic ions, J. Photochem. Photobiol. A Chem. 108 (1) (1997) 37–44, https://doi.org/10.1016/S1010-6030(96)04411-5.

[63] R.A. Burns, J.C. Crittenden, D.W. Hand, V.H. Selzer, L.L. Sutter, S.R. Salman, Effect of inorganic ions in heterogeneous photocatalysis of TCE, J. Environ. Eng. 125 (1) (1999) 77–85.

[64] M. Lindner, D.W. Bahnemann, B. Hirthe, W.D. Griebler, Solar water detoxification: novel TiO_2 powders as highly active photocatalysts, J. Sol. Energy Eng. Trans. ASME. 119 (1997) 120–125, https://doi.org/10.1115/1.2887890.

[65] P. Calza, E. Pelizzetti, Photocatalytic transformation of organic compounds in the presence of inorganic ions, in: Pure Appl. Chem., Walter de Gruyter GmbH, 2001: pp. 1839–1848. https://doi.org/10.1351/pac200173121839.

[66] C. Guillard, E. Puzenat, H. Lachheb, A. Houas, J.M. Herrmann, Why inorganic salts decrease the TiO_2 photocatalytic efficiency, Int. J. Photoenergy 7 (2005) 1–9, https://doi.org/10.1155/S1110662X05000012.

[67] F. Sunada, A. Heller, Effects of water, salt water, and silicone overcoating of the TiO_2 photocatalyst on the rates and products of photocatalytic oxidation of liquid 3-octanol and 3-octanone, Environ. Sci. Technol. 32 (2) (1998) 282–286, https://doi.org/10.1021/es970523f.

[68] F. Pellegrino, L. Pellutiè, F. Sordello, C. Minero, E. Ortel, V.D. Hodoroaba, V. Maurino, Influence of agglomeration and aggregation on the photocatalytic activity of TiO_2 nanoparticles, Appl. Catal. B Environ. 216 (2017) 80–87, https://doi.org/10.1016/j.apcatb.2017.05.046.

[69] E. Dworniczek, G. Plesch, A. Seniuk, R. Adamski, obert Michal, Photo-catalytic inactivation of an Enterococcus biofilm: the anti-microbial effect of sulphated and europium-doped titanium dioxide nanopowders, FEMS Microbiol. Lett. 363 (2016) 51. https://doi.org/10.1093/femsle/fnw051.

[70] S. Yu, T. Lin, W. Chen, Photocatalytic inactivation of particle-associated Escherichia coli using UV/TiO2, RSC Adv. 4 (2014) 31370–31377, https://doi.org/10.1039/C4RA04061A.

[71] J. Yan, B.L. Bassler, Surviving as a community: antibiotic tolerance and persistence in bacterial biofilms, Cell Host Microbe. 26 (1) (2019) 15–21.

[72] H. AM, N. AC, M. RE, S. PR, S. WH, M. L, S. GD, H. PA, Dispersion of TiO_2 nanoparticle agglomerates by Pseudomonas aeruginosa, Appl. Environ. Microbiol. 76 (2010) 7292–7298. https://doi.org/10.1128/AEM.00324-10.

[73] H. M, S. M, Functions of ROS in Macrophages and Antimicrobial Immunity, Antioxidants (Basel, Switzerland). 10 (2021) 1–39. https://doi.org/10.3390/ANTIOX10020313.

[74] H. Choi, Z. Yang, J.C. Weisshaar, Oxidative stress induced in E. coli by the human antimicrobial peptide LL-37, PLOS Pathog. 13 (6) (2017) e1006481, https://doi.org/10.1371/journal.ppat.1006481.

[75] R. van Grieken, J. Marugán, C. Pablos, L. Furones, A. López, Comparison between the photocatalytic inactivation of gram-positive E. faecalis and gram-negative E. coli faecal contamination indicator microorganisms, Appl. Catal. B Environ. 100 (1-2) (2010) 212–220.

[76] D. Venieri, E. Chatzisymeon, M.S. Gonzalo, R. Rosal, D. Mantzavinos, Inactivation of Enterococcus faecalis by TiO2-mediated UV and solar irradiation in water and wastewater: culture techniques never say the whole truth, Photochem. Photobiol. Sci. 10 (2011) 1744–1750, https://doi.org/10.1039/C1PP05198A.